Journal of Materials Chemistry B

Accepted Manuscript

ROYAL SOCIETY OF CHEMISTRY

rsc.li/materials-b

View Article Online
DOI: 10.1039/C6TB03062A

Journal Name

REVIEW

Electron microscopy for inorganic-type drug delivery nanocarriers for antitumoral applications: What is possible to see?

A. Baeza,[a] R. R. Castillo,[a] A. Torres-Pardo,[b] J. M. González-Calbet[b] and M. Vallet-Regí*[a]

Received 00th January 20xx,
Accepted 00th January 20xx

DOI: 10.1039/x0xx00000x

www.rsc.org/

The use of nanoparticles able to transport drugs, in a selective and controlable manner, directly to diseased tissues and cells have improved the therapeutic arsenal for addressing unmet clinical situations. In the recent years, a vast number of nanocarriers with inorganic, organic, hybrid and even biological nature have been developed, expecially for their application in oncology fied. The exponential growing in the nanomedicine field would not have been possible without the also rapid expansion of electron microscopy techniques, which allow a more precise observation of nanometric objects. The use of these techniques provides a better understanding of the key parameters which rule their synthesis and behavior. In this review, the recent advances performed in the application of inorganic nanoparticles for clinical uses and the role which has played electron microscopy will be presented.

Introduction

Inspired by the visionary speech of Richard Feynman in 1959 at the annual meeting of the American Physical Society, scientists with different backgrounds have struggled to understand the principles of the behaviour of the matter in nanometer scale. Thanks to their efforts, nanotechnology is nowadays a well-established science and has significantly contributed to the development of diverse fields such as materials science, physics, chemistry and medicine, among others. Nanoparticles are currently at the roots of a variety of application domains, spanning from catalysis and nanoelectronics, to biomedicine or healthcare. In all cases, their functionality is tightly related to the ultimate structural and compositional details, as well as to their interactions with other particles in multicomponent-type materials. The progress of this science would not have been possible without the parallel development of the electron microscopy, which has given the scientific community the opportunity to directly visualize the nanometer world. The broad range of electron microscopy techniques (imaging techniques, analytical spectroscopies, tomography, gas or liquid *in situ* experiments …) currently provide the means to reveal at the finest spatial scale, down to sub-Angstrom, the 2D and 3D information required to monitor the structure and functionalization of such nanometric systems as well as to rationalize their behaviour. In the last decades, the use of nanoparticles in medicine has provided new weapons to fight unmet diseases[1] and also helped in the development of more accurate diagnosis tools.[2] Their nanometric size allows a close interaction with their biological targets such as cells, bacteria or viruses, resulting in an improved therapeutic response with reduced side effects.[3] Simply with the fact to encapsulate a drug within a nanoparticle produces several interesting advantages such as enhanced circulation time in comparison with the free drug, higher drug concentration in the target zone and the possibility to employ lipophilic drugs, which is the case of many antitumoral compounds.[4] The external surface of these carriers can be decorated with synthetic or natural biomolecules in order to detect the desired target, either a diseased tissue[5] or cell,[6] enhancing the selectivity of the nanocarrier. Additionally, these nanodevices can be engineered with stimuli-responsive properties in order to release their payloads only in the presence of certain stimuli which reduce even more the side toxicity of the therapy. These stimuli could be specific to the treated disease as pH alterations, presence of enzymes or molecules, or can be externally applied such as light, magnetic fields or ultrasounds, among others.[7] For the development of these smart materials, recent advances in electron microscopy[8,9] have played an essential role allowing a precise visualization of both the particle morphology itself and its cargo and external functionalization. Due to the vast number of nanodevices reported, in this review, a brief description of the recent advances carried out in the development of some of the most promising inorganic nanocarriers as mesoporous silica nanoparticles, metal-organic nanoparticles and graphene nanosheets, as examples of materials with rigid, hybrid and soft nature, respectively will be presented. Along this review, the role of electron microscopy in the nanoparticle characterization, as well as in the understanding of the interactions with their biological targets will be described.

[a] Dpto. Química Inorgánica y Bioinorgánica. Facultad de Farmacia, Universidad Complutense de Madrid. Plaza Ramon y Cajal s/n. Instituto de Investigación Sanitaria Hospital 12 de Octubre i+12, Centro de Investigación Biomédica en Red de Bioingeniería, Biomateriales y Nanomedicina (CIBER-BBN). Madrid, Spain.
[b] Dpto. de Química Inorgánica Facultad de Químicas, Universidad Complutense de Madrid, Madrid, Spain

View Article Online
DOI: 10.1039/C6TB03062A

Inorganic nanocarriers for drug delivery applications.

Inorganic nanoparticles, especially those with a porous nature, have emerged as powerful materials for drug delivery applications. One relevant characteristic of these materials is their high loading capacity; with external surface areas ranging from values between 500-10,000 $m^2 \cdot g^{-1}$. Additionally, their pore network is easily tuneable, which allows the transport of molecules with very different sizes, from macromolecules as proteins, enzymes, DNA or RNA strands to small molecules as antibiotics or cytotoxic compounds, among others. Both features allow the delivery of high number of therapeutic species with very different nature which is valuable for combination antitumoral therapy.[10,11] Besides these properties, inorganic carriers present other interesting characteristics such as low toxicity and immunogenicity, easy and cheap production and high chemical and mechanical resistance, which make them excellent materials for clinical applications. However, due to the lack of flexibility which is commonly exhibited by the major part of inorganic nanocarriers, their diffusion within the living tissues is specially hampered. This fact compromise the nanocarrier distribution along the affected tissue and therefore, it diminishes the efficacy of the therapy. Despite this fact, the use of inorganic nanoparticles in medicine has been widely studied and several strategies have been proposed in order to exploit their advantages alleviating their limitations, as it will be described along this review.

Mesoporous Silica Nanoparticles (MSNs).

There is a wide arsenal of synthetic methods for the production of MSNs with different morphologies such as spherical, rod, hollow or rattle, among others.[12-15] Particle morphology plays a key role in the cell internalization process. Therefore, its characterization by Scanning Electron Microscopy (SEM)[9] –to monitor the surface fine structure and morphology– and Transmission Electron Microscopy (TEM)[8] –to have access to the 3D morphology, the crystalline structure and the local chemical composition– is essential in order to get a proper insight of the biological properties of these systems.[16,17] Pore diameter is other important feature of MSNs. As in the previous case, there are many different synthetic methods which allow obtaining materials with pores from 2 nm, suitable for the delivery of small therapeutic agents (antibiotics, cytotoxic compounds, vitamins, etc.) to a few tens of nanometres, required for the transport of macromolecules such as proteins or nucleotide strands. Additionally, the pore distribution and order can also be controlled; thus, MSNs can be obtained with parallel,[18] radial,[19] fibrous[20] or dendritic pore structures,[21] being all of them clearly observable by TEM. Recently, Yu *et al.* have described the synthesis of beautiful MSNs with a core–cone pore structure, similar to the flower *dahlia hortensis*, which presents narrowly packed curved petals surrounding a central core.[22] In this work, the authors employed electron tomography technique to describe the original morphology. Electron tomography records a series of images in which the orientation of the specimen is varied relative to the incident beam.[23] As a result, the image series contains all the information required to perfectly define the 3D structure of the novel structure. The performed study revealed that, besides its beauty, this system had an astonishing high pore volume of 2.59 $cm^3 \cdot g^{-1}$ and pores diameters of 45 nm, which also allowed the shipping of big proteins (>100KDa) in large number. The silica network can be also altered through substitution of Si atoms by other heteroatoms such as Al, Sn, Fe, Nb or Ti in order to modify the chemical nature of the material and therefore, altering their catalytic or dug release properties.[24] The determination of the Si/Heteroatom substitution grade and the exact location of the doping elements in the silica network can be analysed by spectroscopic techniques such energy dispersive X-ray (EDX) and electron energy loss spectroscopy (EELS), associated to TEM operating in scanning mode (Scanning TEM, STEM). In STEM mode, a small electron beam probe is focused and then raster over the sample while the inelastic processes as the result of the interaction between the incident electron beam and the matter allows the spatially resolved EELS or EDX elemental mapping for the identification and quantification of the elements present in the sample.[8] In 2010, Vallet-Regí and co-workers were pioneers in the detection of drug molecules confined within the pore network of MSNs.[25] In this work, pore channels were loaded with zoledronate, a drug widely employed in different bone pathologies. The material was studied by STEM operating microscope with spherical aberration corrector in the probe (JEM-ARM200F) coupled with a high energy resolution EELS spectrometer. The exceptional spatial resolution (0.08 nm) and the analytical capability of this instrumentation allowed performing spatially resolved analysis to detect the presence of drug inside the pores. As it is showed in Figure 1a, when the electron beam was perpendicularly oriented to the mesoporous channels, only Si and O were detected by EELS analysis, which was in accordance with the composition of silica walls. In opposition, if the electron beam was parallel to the channels (Figure 1b), EELS analysis evidenced C and N located within the mesopores which corresponds to the presence of zoledronate. This work supposed the first evidence that could be possible to determine the presence of organic molecules within the pore network of inorganic materials employing only electron microscopy.

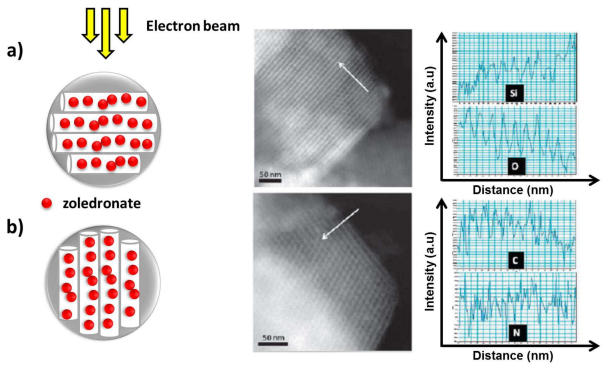

Fig. 1 Detection of drugs loaded within MSNs channels by EELS with mesoporous channels a) perpendicular or b) parallel to electron beam. Si, O, C and N lines correspond to the intensity of the EELS Si-K; O-K; C-K and N-K edges, respectively.

View Article Online
DOI: 10.1039/C6TB03062A

In addition to loading the nanocarriers with therapeutic agents, smaller nanoparticles such as gold,[26] iron oxide,[27] silver nanocrystals,[28] and many others, can be trapped within the mesoporous silica matrix. Thus, thanks to the presence of these metallic particles, photothermal properties, magnetic hyperthermia or antibacterial ability can be respectively added enhancing the potential clinical application of these devices. Metal-particles coated with the mesoporous silica shell can be clearly observed by TEM imaging –which image contrast is highly sensitive to the mass contrast– as well as by STEM using High Angle Annular Field imaging technique –which image contrast is highly sensitive to the atomic number–. In both, the different atomic number between the heavy metal atoms in comparison with the silica counterpart provides a clear difference in the contrast among both materials that permits perfectly identifying the core-shell composite. Additionally, the particle composition can be analysed by EDX-STEM or EELS-STEM with highly spatial resolution and their crystallinity degree can be further determined by high-resolution TEM analysis. Zink *et al.* have developed a hybrid dual core MSNs device which encapsulates in the same carrier superparamagnetic iron oxide nanoparticles (SPIONs) and Yb^{3+}/Er^{3+} doped $NaYF_4$ nanoparticles. This device allowed real-time monitoring of temperature in the particle's surroundings under alternative magnetic field exposition.[29] SPIONs generated heat once the magnetic field is applied while Yb^{3+}/Er^{3+}-doped $NaYF_4$ nanoparticles act as nanothermometer because its luminescence is strongly dependent on the surrounding temperature. Therefore, measuring the luminescence change when the magnetic field is applied it is possible to determine with a high precision degree the temperature in the particle surrounding which is of paramount importance for the development of magnetic responsive devices.[30] This device was characterized by combining high-resolution TEM, STEM and EDX mapping analysis, showed that 70% of hybrid MSNs presented 1:1 ratio between SPIONs and Yb^{3+}/Er^{3+} doped $NaYF_4$ nanoparticle with an average distance between them of around 8-9 nm, which indicated the excellent performance of the synthetic procedure. Unfortunately, the encapsulation of metallic particles within MSNs could result in a significant loading capacity reduction and therefore, a limited therapeutic capacity in the case of drug delivery nanodevices. Recently, Li *et al.*[31] have developed Janus Silver-MSNs which combine the surface plasmon resonance (SPR) properties of silver with the excellent loading capacity of MSNs. Characterization by SEM, TEM and EDX mapping confirmed that this device presented a bullet-based Janus structure of approximately 300 nm, in which only one silver particle was embedded per silica rod.

In any case, the use of pure inorganic materials as drug carriers for clinical applications is very limited. The intravenous administration of naked inorganic particles usually leads to a rapid elimination as a consequence of their capture by Mononuclear Phagocyte System (MPS). MPS has evolved during millions of years in order to recognize foreign agents (as these particles) and orchestrates their elimination.[32] The external surface of these materials must be decorated with (bio)-organic moieties in order to avoid the premature capture of these carriers. The most common strategy for enhancing their circulation time consists in the attachment of hydrophilic polymers such as polyethylene glycol (PEG)[33] or zwitterionic polymers.[34] The presence of these polymer chains on the nanocarrier surface hampers the adsorption of opsonins, which are proteins that trigger the clearance pathway by MPS. Moreover, the attachment of hydrophilic polymers also enhances the colloidal stability of MSNs in biological fluids,[35] which is a very important parameter due to particle aggregation not only reduces the circulation time within the blood stream but it can also produce lethal embolism.[36] The introduction of PEG chains on the particle surface is difficult to be confirmed by electron microscopy techniques because these polymers are usually grafted in low amount. Additionally, the sensitive nature of organic nature against electron beams complicates even more the visualization by these techniques. For this reason, the grafting step was monitored using massive spectroscopic techniques such as nuclear magnetic resonance (NMR) or Fourier-transform infrared (FTIR).

Among the different types of MSNs, MCM-41 is one of the most widely employed types for clinical applications due to its unique pore structure. This pore network is characterized by the presence of parallel pores of 2-5 nm without interconnections between them. Once the nanocarrier is loaded with the therapeutic species, it is possible to block the drug departure through the attachment of organic or inorganic moieties on the pore outlets which act as caps. Therefore, stimuli-responsive materials can be easily synthesized grafting these caps through reversible or cleavable bonds sensitive to adequate stimuli.[37] This stimuli-responsive property is especially important when the transported drug is toxic or can induce the apparition of severe side effects, as is the case of, for example, antitumoral compounds, some anti-inflammatory drugs or certain antibiotics. Nanocrystals such as SPIONs,[38] gold[39] or CdS,[40] among others, have been grafted on MSNs surface through cleavable bonds in order to control the drug release behaviour (Figure 2a). In these cases, the attached gatekeepers were clearly observable by TEM thanks to the presence of the heavy atoms (Fe, Au and Cd, respectively). However, if the employed gatekeepers do not present these heavy elements as is the case of the use of cyclodextrins,[41] DNA strands[42] or small molecules,[43] their detection by electron microscopy techniques is harder and requires the use spectroscopic techniques such as solid-state NMR or Fourier-Transform infrared spectroscopy (FTIR), among others (Figure 2b).

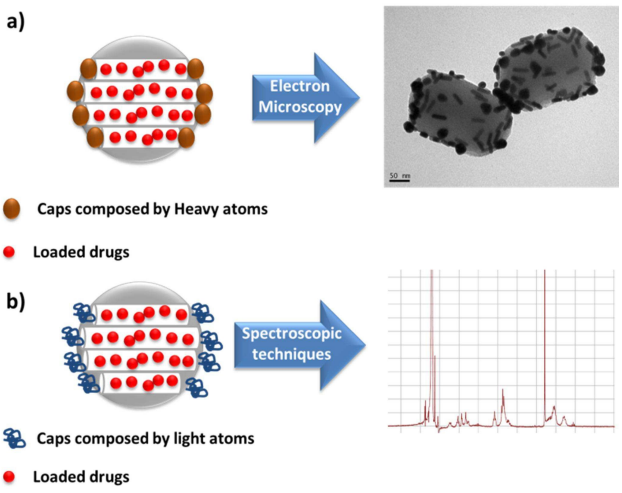

Fig. 2 Characterization techniques available for drug loaded stimuli-responsive MSNs sealed with caps which present a) heavy atoms and b) light atoms (C, H, N and O)

Other available strategy for controlling the drug departure process is to coat the MSNs surface with polymers able to experience either conformational changes in response to certain stimuli or be

View Article Online
DOI: 10.1039/C6TB03062A

degraded in the presence to some conditions. Thus, thermosensitive polymers based on polyNIPAM have been widely employed in order to provide devices able to release their cargo once the temperature reaches certain value.[44] When the temperature is maintained below the transition temperature, the polymer shell is completely hydrated acting as a diffusion barrier which hampers the drug release, whereas if the temperature exceeds this value, the polymer suffers a collapse allowing the drug release. The thickness of the polymer layer is sufficiently wide (a few nanometres) to allow its visualization employing TEM. Interestingly, if the density of the polymer shells which envelopes the MSN is low and the polymer chains are not cross-linked between them, the release behavior is just the opposite. In this case, the polymer layer in its hydrated state cannot avoid the drug departure but, when the temperature reaches the transition temperature, some of the collapsed polymer chains blocks the pore outlet avoiding the drug leakage. [45] In order to increase the image contrast between the silica and the polymer layer, different electro-opaque staining agents such as uranyl acetate or phosphotungstic acid can be employed. These agents present variable affinities by the organic layer, leading to highly or poorly contrasted micrographs, respectively. The same staining agents have also been employed to visualize other organic-based coatings for MSNs such as lipid bilayers[46] or biopolymers,[47] among others. Other polymers have been produced in order to exploit different stimulus which trigger the drug release. Thus, polymers which contain functional groups sensitive to ultrasounds,[48] enzymes,[49] pH[47] or redox species[50] have been attached on MSNs surface in order to provide the responsive capacity to these stimulus, respectively.

Despite the nice performance exhibited by these devices in *in vitro* tests, the achievement of a perfect capping which completely avoids the premature release of the housed therapeutic agents is difficult, especially when they are exposed to a more complex environment as is the inner of a living system. An interesting alternative to the transport of active therapeutic agents consist in the use of prodrugs. Vallet-Regí *et al.* have developed a hybrid MSNs able to generate *in situ* cytotoxic compounds once is accumulated within tumoral cells.[51] The core of this device consists in amino-functionalized MSNs able to retain indol-3-acetic acid (IAA), a plant hormone completely harmless for humans. The enzyme responsible for the transformation of IAA into cytotoxic species, *horseradish peroxidase* (HRP), which is also innocuous, was previously coated with a thin polymeric shell and then, was grafted on the MSNs surface. This shell preserves its enzymatic activity at the same time that increases its resistance. These grafted enzyme nanocapsules were clearly observed by TEM employing phosphotungstic acid as staining agent showing a homogeneous distribution over the entire particle surface (Figure 3). This device was efficiently uptaken by different tumoral cells (neuroblastoma and leukaemia) and once inside them, the sustained release of IAA followed by its transformation into cytotoxic species led to cell destruction.

Metal-Organic Nanoparticles (MONs)

MONs are coordination polymers built using metal-ligand bonds and constitute other promising family of materials for drug delivery applications. Their potential is due to their particular properties such as: i) high synthetic versatility regarding composition, shape, size, porosity and chemical properties, ii) high loading capacity, iii) biodegradability due to the labile metal bonds and iv) the complementary properties provided by the presence of metal ions (magnetic, electronic or optical) which can be exploited for the production of theranostics devices thanks to the combination of high capacity to transport and release therapeutic agents with imaging or diagnosis properties.

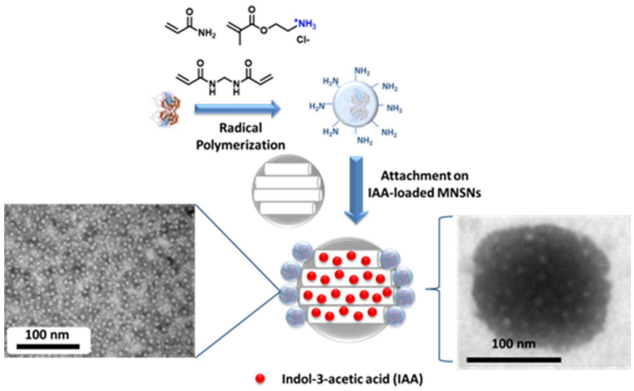

Fig. 3 MSNs coated with HRP nanocapsules. Left TEM image shows HRP nanocapsules alone and right TEM image shows the complete system, both stained with phosphotungstic acid.

Two different categories can be differentiated within the MON family: nanoscale coordination polymers (NCPs) which present amorphous structure and nanoscale metal–organic frameworks (NMOFs) that exhibit ordered porous structure.[52] The last group present very high loading capacity as a consequence of the significant porosity of these materials. The loading capacity is lower in the first group but in some cases these carriers can encapsulate drugs up to 20% of their weight.[53] Additionally, NCPs can be synthesized as porous or hollow-based nanostructures in order to increase their cargo capacity.[54] As in the previous case, a review of the current state of the art of the use of MONs is not intended in this manuscript. Instead, our aim is only to present a few interesting examples of the application of this type of devices in nanomedicine detailing the role of electron microscopy in their characterization. Some reviews which provide a broad panoramic view about the use of these devices for clinical applications can be found elsewhere.[55, 56]

As it has been commented above, NCPs present lower loading capacity than NMOFs but the highly tuneable matrix composition allows the encapsulation of different therapeutic species. NCPs are usually formed by self-assembly process ruled by the nature of metal and bridging ligands. The encapsulation process takes place during the particle formation. The loading yield depends of the interactions between the cargo and the building blocks which forms the particle. So, the control of these interactions, has allowed different species such as fluorophores,[53] cytotoxic drugs[57] and also smaller nanoparticles as SPIONs[58] to be effectively trapped within NCPs. Moreover the bridging ligands themselves could be either therapeutic species or prodrugs, whose release during the degradation process may produce a sustained and significant increase in the loading capacity of those carriers.[59] As in the previous examples, the external surface of these carriers can be decorated with PEG[60] or lipids bilayers[61] in order to enhance their circulation time or to improve their uptake within the target cells. Electron microscopy provides important information about particle

View Article Online
DOI: 10.1039/C6TB03062A

morphology and size distribution. The presence of heavy metal atoms within the particle structure is easily monitored by EDX which would assess the homogeneous distribution of metal ions along the particle. Additionally, due to the fact that the trapped drugs are released as a consequence of the particle degradation, it is possible to test the drug release behaviour through the observation by TEM and SEM of particle erosion during the time.[53] NCPs can be designed in order to present stimuli-responsive drug release properties. As an example, one of the most employed stimuli is pH acidification due to pH-sensitive nature of metal-ligand bonds. Che *et al.* have developed core-shell NCPs able to release different drugs (methotrexate, human glyoxalase I inhibitor or calcein) when the pH drops from physiological conditions (pH = 7.0) to the mild acidic conditions (pH = 5.0)[62] found within the endosomes, lysosomes and also in some tumoral tissues. Therefore, exploiting this pH gradient, the housed drugs can be released once the carriers have entered the target cells or reached the tumoral zone. The carrier was formed by a central core composed by the drugs coordinated with Fe^{2+} or Zn^{2+} cations, coated with a pH-degradable shell of bifunctional 1,4-bis(imidazol-1-ylmethyl)benzene (BIX) bridged by Zn^{2+}atoms. Similar to previous examples, the core-shell structure of this device could be clearly observed by imaging TEM techniques due to the contrast difference between the core and the external shell, which also permitted the exact measurement of the shell thickness. NCPs can exhibit interesting properties by themselves. Indeed, Zhang *et al.* synthesized coordination quantum dots (QD) employing Zn^{2+} and potassium 3,4,9,10-perylenetetracarboxylate as building blocks, which proved to be a suitable material for labelling living cells.[63] The rounded shape morphology of these nanodevices with around 3 nm size was revealed by low magnification TEM imaging and the stabilization of the novel QD formed by the Zn-organic molecule was confirmed by measuring their lattice parameters from high resolution TEM images.

On the other hand, the highly regular pore network of NMOFs makes these materials ideal candidates for drug delivery applications. The pore diameter of MOFs can be engineered in order to house therapeutic agents such as anti-inflammatory,[64] antiarrythmic[65] and antitumoral drugs,[66] to cite just a few examples. In order to be able to fine-tune the loading procedure, it is required a complete characterization of the pore network present in these materials. TEM appears again as an excellent tool to visualize the pore structure in individual particles although, in this case, the damaging effect of the electron beam over the NMOFs needs to be considered. In general, the presence of covalent bonds and a composition involving light elements, result in increased sensitivities to damage by electron beams. These two factors are common to many materials but, in the case of NMOFs, porosity is an extra factor which can promote the loss of sample integrity, because their organic linkers are prone to ionization and the porous configuration tends to diminish its surface area and surface energy by collapsing the structure. Therefore, an extra effort is required on the optimization of the experimental TEM conditions for the characterization of these soft materials generally based on the use of low acceleration voltages and low electron dose. Under these conditions, the morphology and crystallinity of the pore network have been characterized by diffraction and imaging TEM,[67] STEM[68] techniques and even the location of encapsulated particles have been studied by electron tomography.[69]

As in precedent cases, in addition to drug encapsulation, it is also possible to trap other nanoparticles within the metal-organic matrix. Wöll *et al.* have recently reported the synthesis of hierarchically structured metal-organic framework multishells which contains magnetic nanocrystals in the particle core.[70] These devices, built by applying a layer-by-layer synthetic procedure, introduced successively multiple MOF shells with different compositions around a magnetic core. Each MOF shell provided a different property resulting in nanodevices able to perform several tasks at the same time such as multi-imaging agents, magnetic hyperthermia or stimuli-responsive drug release. Here, TEM characterization provided information about the particle thickness increase of each stage of MOF shell formation. In other related example, Duan *et al.* described the synthesis of other core-shell nanodevices composed by metallic cores coated with metal-organic framework shells.[71] This method was based in the previous growth of a polydopamine (PDA) layer around the central metallic nanoparticle. Then, metal-chelating activity provided by catechol groups present in dopamine, direct and controls the growth of the MOF layer affording the formation of discrete core-shell nanoparticles. The excellent adhesive capacity of PDA makes possible the application of this process on a vast number of nanoparticles with different chemical composition, sizes and shapes. For example, this methodology allowed the construction of different MOF shells onto gold, mesoporous silica and polystyrene nanoparticles with spherical or star-shape morphologies thus providing a beautiful collection of hybrid nanodevices which combine different properties (Figure 4). As in the previous materials, EDX mapping provides information about the atomic composition of each layer.[72]

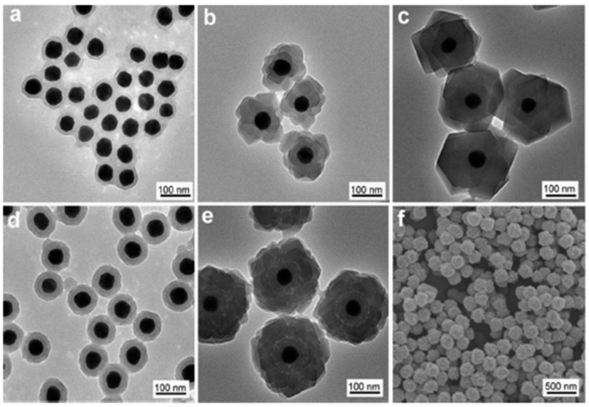

Fig. 4 a-e) TEM images of Au nanoparticles coated with multishells of PDA and MOF (ZIF-8) of different thickness. f) SEM image of Au nanoparticles coated with a multishell of PDA and MOF (ZIF-8). Extracted from reference 71.

Carbon nanoparticles

Carbon nanocarriers can be synthesized in the laboratory mainly in two different forms: carbon nanotubes (CNTs) and graphene oxide (GO) nanosheets. The observation of carbon-based materials by electron microscopy techniques has been traditionally limited by the sensitivity of light elements to electron irradiation. However, the successful implementation of aberration correctors into conventional TEM microscopes has contributed significantly to

View Article Online
DOI: 10.1039/C6TB03062A

improve the spatial resolution and increase the signal to noise ratio while operating at low voltages. These recent progresses offer an unprecedented opportunity to investigate carbon-based nanomaterials, reducing the damage by imaging at voltage of 60–80 kV or even lower.[73]

CNTs are molecular scale tubes formed by graphene sheets rolled up into cylindrical hollow shapes with variable lengths which can vary from hundreds of nanometres to micras. These materials can transport different therapeutic compounds either adsorbed in the external surface or housed in the inner cavity. This cavity can present a diameter of 0.4-2 nm in the case of single-walled carbon nanotubes (SWCNTs) and 2-100 nm for multi-walled carbon nanotubes (MWCNTs). One of the first molecules encapsulated within the inner space of CNTs was other carbon allotrope, the Buckminster fullerene C_{60}.[74] It was observed by high resolution TEM operating at 100 kV, providing nice images of self-assembled chains of fullerenes within CNTs like beans inside a nanometric peapod. The spatial resolution achieved even before the implementation of aberration correctors allowed an accurate measurement of the intermolecular separation of each C_{60} of around 1 nm. Other fullerenes as C_{70} or Ce@C_{82} have been loaded within CNTs with different diameters in order to study the orientation and capacity to perform motions of these molecules within the tubular structure.[75] Many other different molecules have been also encapsulated within CNTs[76] although its preferential loading location is the external surface, which can achieve up to 2500 $m^2 \cdot g^{-1}$. Thus, antitumoral drugs as doxorubicin[77,78] have been adsorbed or covalently grafted on the SWCNTs surface in order to destroy malignant cells.

CNTs aqueous solubility is really poor and therefore, the application of these as drug carriers requires a previous functionalization with polar groups or hydrophilic polymers. As in already discussed materials, these devices can be decorated with different moieties in order to provide useful properties which improve their performance as drug delivery systems.[79] Two interesting reported examples of CNTs as nanomedical platforms are the devices obtained by decoration of their surface with cationic functional groups, which permitted the delivery of DNA[80] or RNA[81] sequences into diseased cells; or the device functionalized with specific peptides able to induce strong immune responses on immune cells, what proved to be an immune activator in vaccination.[82] Additionally, different species can be loaded both in the inner cavity and in the external surface, like CNTs decorated with folate, loaded with doxorubicin and iron oxide nanoparticles.[78] These last particles were formed *in situ* within the inner part of CNTs by encapsulation of Fe^{3+} salts followed by reductive treatment. Observation by TEM confirmed the presence of the metallic nanoparticles of 5-7 nm of diameter at the central cavity. These iron oxide particles enhanced the internalization of the carriers within tumoral areas by magnetic guidance. Similar to the case of MSNs, the end of CNTs can be sealed with different moieties in a reversible way in order to control the release of a drug trapped within the inner section producing a so called nanobottle. Pastorin *et al.* have employed gold nanoparticles as pore caps in order to retain cis-platin within CNTs.[83] Gold nanocaps were functionalized with 1-octadecanethiol and were absorbed by hydrophobic interactions on the nanotube tips as a consequence of their large interaction. The attachment of these caps significantly hampered the drug departure achieving a more sustained drug release profile which improved the cytotoxic capacity of these devices against tumoral cells. The presence of cis-platin inside CNTs was detected by TEM showing high-contrast dots within CNTs could be confirmed as platin species by EDX analysis (Fig 5).

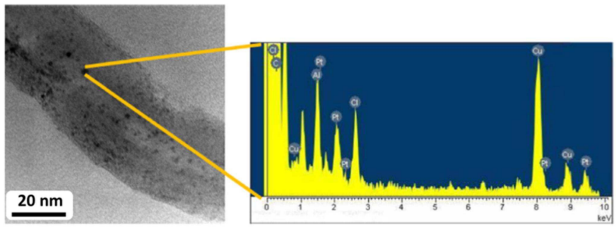

Fig. 5 TEM image of CNTs loaded with cis-platin observable as dark dots and EDX analysis which confirms the presence of platin. Extracted from reference 83.

Graphene is a 2D material formed by one or a few layers of sp^2-hybridized carbon atoms covalently bound forming a honeycomb framework. The atomic structure present in the carbon network exerts great influence in the final properties. As we mentioned above, aberration-corrected TEM[84] and STEM[85] are two powerful techniques to study the graphene framework with extraordinary precision. On the one hand, imaging techniques with atomic resolution provide essential information about the atomic configurations at graphene boundaries or the presence of single atom dopant;[85,86] on the other, their electronic properties can be locally explored by high resolution STEM-EELS.[87] The combination of both, imaging and spectroscopy techniques with atomic resolution permit the direct visualization and identification of changes in the electronic structure of the graphene -therefore in its electro-optic properties- originated by presence of punctual defects or single atom doping and shed light on fundamental scientific questions. Besides its excellent electric and thermal conductivity and its high mechanical strength, highly suitable for materials science, graphene also has really high external surface (2630 $m^2 \cdot g^{-1}$) which makes it an excellent material for drug delivery applications. Nevertheless, due to the poor solubility of graphene in water, it should be oxidized to graphene oxide (GO) in order to increase its dispersability in biological fluids. For this reason, this oxidised form, not only would have better colloidal stability in water but also would present oxygenated functional groups such as hydroxyls, epoxy and carboxylic acid, as recently probed by quantitative STEM-EELS.[88] The presence of these functional groups allows further attachment of different (bio)moieties for improving its performance. Oppositely to pure graphene, which retains drugs by π-π stacking and hydrophobic interactions and therefore only retains efficiently highly hydrophobic drugs, GO is able to transport a wide number of therapeutic agents due to the presence of those hydrophilic groups on its surface.[89] Thus, different compounds have been transported by this type of carrier such as antitumoral agents (doxorubicin[90] and topoisomerase I inhibitors[91]) imaging contrast agents,[92] magnetic nanocrystals[93] or gold nanoparticles,[94] among others. As in previously discussed nanocarriers, PEG has also been employed to modify the surface of GO in order to enhance its circulation time within the blood stream, showing neglictable toxicity in mice models.[95]

GO nanosheets have been employed successfully as pore blockers in combination with porous inorganic nanocarriers. For example, Sailor *et al.* described the synthesis of a core-shell nanodevice formed by mesoporous silicon nanoparticles, with 10 nm-size pores

View Article Online
DOI: 10.1039/C6TB03062A

capable to trap small interfering RNA (siRNAs)[96] within their channels, which were further wrapped with GO nanosheets to slow down the release of the oligonucleotide strands.[97] Additionally, a specific targeting peptide derived from rabies virus glycoprotein was anchored on the GO surface in order to enhance the carrier selectivity for neural cells. TEM images confirmed that GO nanosheets were closely attached on the surface of porous silicon particles which caused a significant reduction of the siRNAs release rate. Graphene also presents a very interesting property for nanomedical applications which is its capacity to generate heat under light irradiation, particularly near-infrared light which besides presents high penetration capacity in living tissues.[98] Thus, the combination of the high loading capacity of GO together with the temperature increase achieved under light irradiation has been used to improve the capacity to destroy tumoral cells of these nanodevices.[99] Ozin *et al.* described in detail the synthetic conditions required for the synthesis of a hybrid nanomaterial formed by graphene oxide and periodic mesoporous silica.[100] The characterization of this nanomaterial by STEM imaging revealed that the GO grid acted as template to guide the formation of mesoporous silica layer, resulting in channels oriented vertically to the carbon plane. This hybrid composite combined the unique properties of graphene with the highly ordered pore network of mesoporous silica. This material has been employed for the treatment of malignant glioma achieving good results in *in vitro* tests.[101] Thus, doxorubicin was loaded within mesoporous silica channels and a specific peptide sequence specific for the receptor chain 2 of interleukin 13 (overexpressed by glioblastoma cells) anchored on the graphene surface. The combination of pH-triggered doxorubicin release when the nanodevice was uptaken by tumoral cells and photothermal capacity when exposed to 808 nm laser beam produced a substantial increase in its cytotoxic capacity, converting this material into a promising candidate for the treatment of this unmet pathology.

Observing the interaction with living systems.

One of the main administration routes of nanomedicines is the injection into the blood stream. Therefore, one of the first living tissues which will contact with the carrier is blood, and this interaction mainly occurs with its cellular components: red blood cells, white blood cells and platelets. The interaction with these cells strongly depends of the composition, surface functionalization, morphology, size and aggregation state of the carrier. White blood cells are the principal components of the immune system and therefore, would lead to particle clearance or triggering immune responses upon interaction with the carrier. Monocytes are cells responsible for the elimination of foreign bodies and usually capture circulating nanoparticles, especially when they are not conveniently functionalized. As mentioned above, particle surface decoration with PEG usually reduces the uptake by these cells as a direct consequence of the opsonin adsorption decrease. A nice example by Arruebo *et al.* studied the uptake of different inorganic nanocarriers by macrophages.[102]

Although TEM imaging techniques could be employed to image nanoparticles inside cells[103] because of the good spatial resolution achieved, the sample preparation requires many treatment processes, some of them -such as centrifugation or cell fixation- can introduce modifications in the organelles, discouraging its use. Nevertheless, such preparation processes are not needed when using SEM. In which, morphological/topological contrast and compositional information are separately obtained by selecting specific types of emitted electrons, known as secondary electrons (with energies smaller than 50 eV) and backscattered electrons (with energies larger than 50 eV); additionally, further compositional information is obtained through EDX analysis. One example of the capabilities of the SEM imaging techniques is the use of secondary electron and backscattered electron imaging to observe nanocarriers on the cell membrane where the semi-quantitative characterization of their atomic composition in the case of metal containing particles was complemented by EDX.[102] Last technical developments in SEM based on the use of field emission guns at low voltages allow the achievement of around 1 nm spatial resolution that satisfies in many cases the spatial resolution requirements for the characterization of the nanoparticle-cell system.[104] In this sense, Havrdova *et al.* employed field emission scanning electron microscopy and the application of gentle beam mode for observing in 3D with ultra-high resolution the nanoparticles into mesenchymal cells allowing the visualization within endosomes (Fig. 6).[105] This technique was also employed for the observation of different types of inorganic nanoparticles (CeO_2, TiO_2 and ZnO) with excellent performance.[106] The presence of heavy atoms allowed obtaining an accurate map of the nanoparticle distribution along the cell. Other contribution to the topic, by Hoogenboom *et al.* described the use of SEM-fluorescence integrated microscope for the visualization of particle endocytosis; in this case there was combined the high resolution achieved with electron microscopy with the great versatility of fluorescent microscopy which provided information about dynamic molecular processes inside the cell.[107]

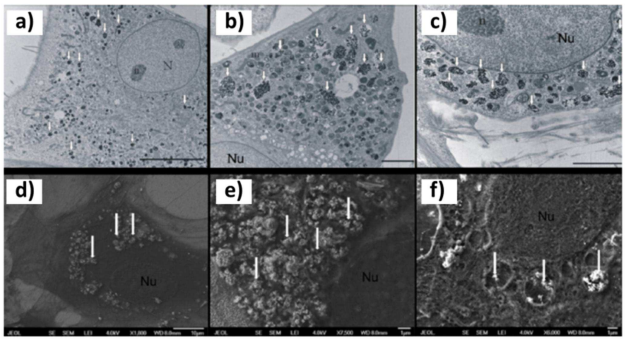

Fig. 6 TEM images of nanocarriers internalized within Mesenchymal cells (white arrows indicate the presence of nanoparticles within endosomes). Extracted from reference 105.

Red Blood cells (RBC) are the major cell component of blood and therefore, to study the particle interaction with these cells is compulsory in order to evaluate in a proper manner the potential toxicity of each carrier. Trewyn *et al.* described the haemolytic activity of MSNs depending on their morphology, size and surface properties.[108] They studied these phenomena and found that small round-shaped MSNs of 100 nm with MCM-41 structure barely disturbed the RBC membrane while larger MSNs (600 nm) with SBA-15 structure provoked a strong disruption in the membrane and thus an enhanced particle internalization which could cause haemolysis. Also, external functionalization played an important role in this process, observing that the higher functionalization grade, the lower interaction with cell membrane. RBC can also be

View Article Online
DOI: 10.1039/C6TB03062A

employed as model of non-phagocytic cells in order to study the potential toxicity of nanoparticles due to the absence of phagocytic receptors on their surface or the actin-myosin system. Gehr *et al.* studied the internalization process of small gold nanoparticles with 25 nm of diameter in RBC employing electron microscopy techniques.[109] In this case the internalization was easily monitored by conventional TEM due to the electro-dense character of gold atoms, observing that the external surface charge did not play any role in the uptake process. Moreover, the particles crossed the membrane when they maintained their discrete nature but they could not be uptaken when aggregated. Interestingly, TEM micrographs showed that these nanoparticles were never surrounded by membranes which could mean that the nanosystems crossed the cell membrane by other mechanism different from endocytosis, such as diffusion, trans-membrane channels or "adhesive interactions". TiO_2 nanoparticle internalization in the same cells was revealed by EELS by monitoring the titanium signal.

In the case of drug delivery carriers, the main goal is to enhance particle uptake in target cells while reducing as much as possible the internalization in healthy cells. This effect can be achieved by grafting targeting agents on the external surface of the nanocarriers. These targeting agents are molecules or biomacromolecules which interact or bind specific membrane receptors located mainly in the target cells. Thus, the presence of targeting groups provokes higher affinity between the nanocarrier and target cell membrane, thus favouring internalization; although particle uptake is a truly complex process which depends of each cell line. But in general, practically all nanoparticles access to the inner cellular space by endocytosis.[110] Endocytosis is a complex energy-dependent process which introduces molecules or nanoparticles within the cell through an invagination process.[111] Once the particle takes contact with the membrane surface, the cell triggers the endocytic mechanism which causes a membrane invagination that wraps the particle. Then, the particle enters into the cytosolic space within a vesicle called endosome. These endosomes can transport the particles to different intracellular organelles, evolve to different structures such as lysosomes which are in charge of the digestion of the uptaked moieties or can be expelled again to the intracellular space in a process called transcytosis. There are different endocytic mechanism being receptor mediated endocytosis the most important one in the case of nanoparticle uptake.[112] In this mechanism, specific moieties which have been anchored on the particle surface recognize cell membrane receptors enhancing the particle affinity by the target cell promoting its internalization. Receptor mediated endocytosis has been exhaustively employed in order to improve the selectivity of the nanocarrier against the tumoral cell, and corresponds the basis of targeted nanoparticles, as was mentioned above. Huang *et al.* studied in detail the influence that exerts the shape of non-functionalized MSNs in the endocytosis process into tumoral cells.[16] They synthesized three types of MSNs with different morphologies, one with spherical shape and two types of rod-shaped particles with different lengths. The internalization process of each particle was monitored by TEM showing that in all cases the particles were first internalized within a vesicle which was merged with endosomes. Finally, the particle escaped from the endosome reaching the cytosolic space. Regarding their biological effect, the authors found that particles with lower aspect:ratio (AR) produced lower interaction with the cells and therefore, altered in lower extension their biological functions. Chan *et al.* studied the effect of size in the nanoparticle internalization process of gold and silver nanoparticles functionalized with antibodies.[113] The authors found that size played a critical role, not only increasing or hindering particle uptake but also in the later location within the cell. The claimed reason was that the number of antibodies able to bind the cell receptors strongly depends on their number and therefore, to particle size, being higher for larger particles. On other hand, dissociation constant (K_d) of antibody-receptor system varies inversely with the size. Thus, smaller particles (2 nm) present similar K_d than free antibodies whereas 40 nm particles have around 1000-fold lower K_d which results in a stronger interaction with cell receptor. Other important parameter is the time required for wrapping the particle by the membrane. This time depends on the diffusion rate of cell receptors; this is a bottle-neck process for tiny or huge nanoparticles. For these reason, internalization is optimal with medium-sized particles of 40-50 nm. One of the milestones in the characterization of biological systems is the possibility to observe them in their natural media. Cryo-electron microscopy -in which the biological sample is plunged into a cryogen in order to trap the sample in a thin film of vitreous ice- is one of the most employed techniques for the analysis of biological systems in a near-native, hydrated environment.[114] Although during the last five years the technique has experimented an extraordinary rising as a result of the improvements in microscopes, imaging technologies, and computational approaches,[115] the process captures the biological-nanoparticles system at the moment of freezing, limiting its characterization. In this sense, many efforts have been devoted to the development of TEM instrumentation which allows observation in liquid media. Liquid cell electron microscopy[116] is a novel technique that allows the scientific community to apply the capabilities of the aberration-corrected electron microscopy to the imaging and analysis of liquid-based processes, like in the study of biological materials in liquid water. The measurement cell is usually prepared with two vacuum-tight electron transparent membranes of silicon nitride that isolate the liquid from the vacuum while also confine it into a layer, thin enough for imaging with transmitted electrons. One example of this technique is the recent uptake study of 30 nm gold nanoparticles by living cells.[117] This study employed a continuous flow of buffer solution through the measurement cell in order to maintain cells alive, while the visualization was maintained. Conventional electron microscopy nanoparticle uptake studies mentioned above usually require an extensive conditioning, specimen sectioning treatment or harsh staining procedures that could generate difficult-to-distinguish electro-opaque clusters; thus making difficult to obtain quantitative results free of artefacts. However, liquid cell electron microscopy acquires images from fully hydrated cells which keep their functional structure and therefore, it would be possible to obtain quantitative and accurate information about the three dimensional distribution of the nanoparticles in the entire cell, the total number of uptaked nanoparticles and the number of these particles located within vesicles.

Conclusions and Future Prospects.

The development of multifunctional nanocarriers able to reach specifically diseased cells without affecting healthy ones, and once there, to release their payload in response to an externally applied stimulus or as a consequence of the presence of certain internal stimulus characteristic for the pathological process has received huge attention, especially in oncology field. One of the main reasons of the use of nanoparticles in oncology lies in their passive accumulation within solid tumours (EPR effect). However, this

View Article Online
DOI: 10.1039/C6TB03062A

effect is not as universal as initially thought, but rather exhibits great heterogeneity depending of the tumour type, patient and even the state of the therapy. Thus, the application of a nanocarrier-based therapy is not suitable for all types of cancer and should be carefully considered for each case. Additionally, the interface nanocarrier-biological environment should be studied with more detail. When a nanocarrier contacts with blood, it is immediately covered by a protein shell which form the so called protein corona. This protein shell determines the particle fate because it forms the readable part of the nanodevice for cells. The corona formation is a dynamic process which suffers changes along the nanoparticle journey and more knowledge about this process is required for controlling the selectivity and reproducibility of the nanotherapy. More research is needed in order to create nanomaterials able to overcome these barriers. With no doubt, electron microscopy, in particular TEM with spatial and analytical resolution at the atomic scale, is one of the essential tools required to gain knowledge needed for improving the efficacy of nanomedicines. Unfortunately, the resolution benefits of electron microscopy, SEM and TEM, are associated with the challenge of preserving the functionalized nanocarriers as well as their biological environment during the experiments. The successful technological development of low voltage microscopy with high resolution during last years has critically improved the stability of the inorganic nanocarriers and the biological systems during their observation and local spectroscopic analysis, seeding light to still unanswered scientific problematic. Nevertheless, the future of the electron microscopy in nanomedicine is necessary linked to the complete development of the microscopy in the liquid state. The challenge of visualizing living systems in their native liquid state offers the possibility of obtaining high-resolution information while avoiding material damage as a result of the sample preparation, although a lot of work has to be still made on understanding the electron dose effects to evaluate which biological functions are preserved or missing during the TEM observation.

Acknowledgements

This work was supported by the European Research Council (Advanced Grant VERDI; ERC-2015-AdG Proposal No. 694160) and Spanish Government through the projects MAT2015-64831-R and MAT2014-58729-JIN.

Notes and references

1 A. Ediriwickrema and W. M. Saltzman, *ACS Biomater. Sci. Eng.*, 2015, **1**, 64–78.
2 H. Chen, Z. Zhen, T. Todd, P. K. Chu, and J. Xie, *Mater. Sci. Eng. R Reports*, 2013, **74**, 35–69.
3 A. K. Mitra, V. Agrahari, A. Mandal, K. Cholkar, C. Natarajan, S. Shah, M. Joseph, H. M. Trinh, R. Vaishya, X. Yang, Y. Hao, V. Khurana, and D. Pal, *J. Control. Release*, 2015, **219**, 248–268.
4 M. W. Tibbitt, J. E. Dahlman, and R. Langer, *J. Am. Chem. Soc.*, 2016, **138**, 704–717.
5 J. Mai, Y. Huang, C. Mu, G. Zhang, R. Xu, X. Guo, X. Xia, D. E. Volk, G. L. Lokesh, V. Thiviyanathan, D. G. Gorenstein, X. Liu, M. Ferrari, and H. Shen, *J. Control. Release*, 2014, **187**, 22–29.
6 L. D. Field, J. B. Delehanty, Y. Chen, and I. L. Medintz, *Acc. Chem. Res.*, 2015, **48**, 1380–1390.
7 S. Mura, J. Nicolas, and P. Couvreur, *Nat. Mater.*, 2013, **12**, 991–1003.
8 R. Brydson, Ed., *Aberration-Corrected Analytical Transmission Electron Microscopy*, John Wiley & Sons, Ltd, Chichester, UK, 2011.
9 M. Suga, S. Asahina, Y. Sakuda, H. Kazumori, H. Nishiyama, T. Nokuo, V. Alfredsson, T. Kjellman, S. M. Stevens, H. S. Cho, M. Cho, L. Han, S. Che, M. W. Anderson, F. Schüth, H. Deng, O. M. Yaghi, Z. Liu, H. Y. Jeong, A. Stein, K. Sakamoto, R. Ryoo, and O. Terasaki, *Prog. Solid State Chem.*, 2014, **42**, 1–21.
10 L. Ma, M. Kohli, and A. Smith, *ACS Nano*, 2013, **7**, 9518–9525.
11 R. R. Castillo, M. Colilla, and M. Vallet-Regí, *Expert Opin. Drug Deliv.*, 2016 (doi: 10.1080/17425247.2016.1211637).
12 M. Vallet-Regí, A. Rámila, R. P. del Real and J. Perez-Pariente, *Chem. Mater.*, 2001, **13**, 308-311.
13 M. Vallet-Regí, F. Balas and D. Arcos, *Angew. Chem. Int. Ed.*, 2007, **46**, 7548-7558.
14 S. Wu, X. Huang, and X. Du, *J. Mater. Chem. B*, 2015, **3**, 1426–1432.
15 L. Li, Y. Guan, H. Liu, N. Hao, T. Liu, X. Meng, C. Fu, Y. Li, Q. Qu, Y. Zhang, S. Ji, L. Chen, D. Chen, and F. Tang, *ACS Nano*, 2011, **5**, 7462–7470.
16 X. Huang, X. Teng, D. Chen, F. Tang, and J. He, *Biomaterials*, 2010, **31**, 438–448.
17 T. Yu, A. Malugin, and H. Ghandehari, *ACS Nano*, 2011, **5**, 5717–5728.
18 Y. Zhao, J. L. Vivero-Escoto, I. I. Slowing, B. G. Trewyn, and V. S.-Y. Lin, *Expert Opin. Drug Deliv.*, 2010, **7**, 1013–1029.
19 K. Möller, J. Kobler, and T. Bein, *Adv. Funct. Mater.*, 2007, **17**, 605–612.
20 V. Polshettiwar, D. Cha, X. Zhang, and J. M. Basset, *Angew. Chem. Int. Ed.*, 2010, **49**, 9652–9656.
21 D. Shen, J. Yang, X. Li, L. Zhou, R. Zhang, W. Li, L. Chen, R. Wang, F. Zhang, and D. Zhao, *Nano Lett.*, 2014, **14**, 923–932.
22 C. Xu, M. Yu, O. Noonan, J. Zhang, H. Song, H. Zhang, C. Lei, Y. Niu, X. Huang, Y. Yang, and C. Yu, *Small*, 2015, **11**, 5949–5955.
23 P. A. Midgley and R. E. Dunin-Borkowski, *Nat. Mater.*, 2009, **8**, 271–280.
24 J. Chen, F. Lu, and J. Xu, *RSC Adv.*, 2015, **5**, 5068–5071.
25 M. Vallet-Regi, M. Manzano, J. M. Gonzalez-Calbet, and E. Okunishi, *Chem. Commun.*, 2010, **46**, 2956–2958.
26 H. Li, L.-L. Tan, P. Jia, Q.-L. Li, Y.-L. Sun, J. Zhang, Y.-Q. Ning, J. Yu, and Y.-W. Yang, *Chem. Sci.*, 2014, **5**, 2804–2808.
27 E. Ruiz-Hernández, A. Baeza, and M. Vallet-Regí, *ACS Nano*, 2011, **5**, 1259–1266.
28 Y. Wang, X. Ding, Y. Chen, M. Guo, Y. Zhang, X. Guo, and H. Gu, *Biomaterials*, 2016, **101**, 207–216.
29 J. Dong and J. I. Zink, *ACS Nano*, 2014, **8**, 5199–5207.
30 E. Guisasola, A. Baeza, M. Talelli, D. Arcos, M. Moros, J. M. D. La Fuente, M. Vallet-Regí, *Langmuir*, 2015, **31**, 12777–12782.
31 D. Shao, X. Zhang, W. Liu, F. Zhang, X. Zheng, P. Qiao, J. Li, W. Dong, and L. Chen, *ACS Appl. Mater. Interfaces*, 2016, **8**, 4303–4308.
32 J. W. Nichols and Y. H. Bae, *Nano Today*, 2012, **7**, 606–618.
33 A. S. Karakoti, S. Das, S. Thevuthasan, and S. Seal, *Angew. Chemie - Int. Ed.*, 2011, **50**, 1980–1994.
34 J. T. Sun, Z. Q. Yu, C. Y. Hong, and C. Y. Pan, *Macromol. Rapid Commun.*, 2012, **33**, 811–818.
35 Y. S. Lin, K. R. Hurley, and C. L. Haynes, *J. Phys. Chem. Lett.*, 2012, **3**, 364–374.
36 S. P. Hudson, R. F. Padera, R. Langer, and D. S. Kohane, *Biomaterials*, 2008, **29**, 4045–4055.
37 A. Baeza, M. Colilla, and M. Vallet-Regí, *Expert Opin. Drug Deliv.*, 2015, **12**, 319–337.
38 S. Giri, B. G. Trewyn, M. P. Stellmaker, and V. S.-Y. Lin, *Angew. Chemie Int. Ed.*, 2005, **44**, 5038–5044.

View Article Online
DOI: 10.1039/C6TB03062A

39 F. Torney, B. G. Trewyn, V. S.-Y. Lin, and K. Wang, *Nat. Nanotechnol.*, 2007, **2**, 295–300.
40 C.-Y. Lai, B. G. Trewyn, D. M. Jeftinija, K. Jeftinija, S. Xu, S. Jeftinija, and V. S.-Y. Lin, *J. Am. Chem. Soc.*, 2003, **125**, 4451–4459.
41 J. Liu, Z. Luo, J. Zhang, T. Luo, J. Zhou, X. Zhao, and K. Cai, *Biomaterials*, 2016, **83**, 51–65.
42 P. Zhang, F. Cheng, R. Zhou, J. Cao, J. Li, C. Burda, Q. Min, and J. J. Zhu, *Angew. Chemie - Int. Ed.*, 2014, **53**, 2371–2375.
43 D. He, X. He, K. Wang, J. Cao, and Y. Zhao, *Langmuir*, 2012, **28**, 4003–4008.
44 A. de Sousa, D. A. Maria, R. G. de Sousa, and E. M. B. de Sousa, *J. Mater. Sci.*, 2010, **45**, 1478–1486.
45 E. Guisasola, A. Baeza, M. Talelli, D. Arcos and M. Vallet-Regí. *RSC Adv.*, 2016, **6**, 42510–42516.
46 L. Wang, L. Wu, S. Lu, L. Chang, I. Teng, C. Yang, and J. A. Ho, *ACS Nano*, 2010, **4**, 4371–4379.
47 M. Martínez-Carmona, D. Lozano, M. Colilla, and M. Vallet-Regí, *RSC Adv.*, 2016, **6**, 50923–50932.
48 J. L. Paris, M. V. Cabañas, M. Manzano, and M. Vallet-Regí, *ACS Nano*, 2015, **9**, 11023–11033.
49 A. Bernardos, L. Mondragón, E. Aznar, M. D. Marcos, R. Martínez-Máñez, F. Sancenón, J. Soto, J. M. Barat, E. Pérez-Payá, C. Guillem, and P. Amorós, *ACS Nano*, 2010, **4**, 6353–6368.
50 Z. Luo, K. Cai, Y. Hu, L. Zhao, P. Liu, L. Duan, and W. Yang, *Angew. Chemie - Int. Ed.*, 2011, **50**, 640–643.
51 A. Baeza, E. Guisasola, A. Torres-Pardo, J. M. González-Calbet, G. J. Melen, M. Ramirez, and M. Vallet-Regí, *Adv. Funct. Mater.*, 2014, **24**, 4625–4633.
52 C. He, D. Liu, and W. Lin, *Chem. Rev.*, 2015, **115**, 11079–11108.
53 I. Imaz, M. Rubio-Martínez, L. García-Fernández, F. García, D. Ruiz-Molina, J. Hernando, V. Puntes, and D. Maspoch, *Chem. Commun.*, 2010, **46**, 4737–4739.
54 M. Hu, A. A. Belik, M. Imura, and Y. Yamauchi, *J. Am. Chem. Soc.*, 2013, **135**, 384–391.
55 P. Horcajada, R. Gref, T. Baati, P. K. Allan, G. Maurin, P. Couvreur, G. Férey, R. E. Morris, and C. Serre, *Chem. Rev.*, 2012, **112**, 1232–1268.
56 F. Novio, J. Simmchen, N. Vázquez-Mera, L. Amorín-Ferré, and D. Ruiz-Molina, *Coord. Chem. Rev.*, 2013, **257**, 2839–2847.
57 F. Novio, J. Lorenzo, F. Nador, K. Wnuk, and D. Ruiz-Molina, *Chem. - A Eur. J.*, 2014, **20**, 15443–15450.
58 M. Borges, S. Yu, A. Laromaine, A. Roig, S. Suárez-García, J. Lorenzo, D. Ruiz-Molina, and F. Novio, *RSC Adv.*, 2015, **5**, 86779–86783.
59 W. J. Rieter, K. M. Pott, K. M. L. Taylor, and W. Lin, *J. Am. Chem. Soc.*, 2008, **130**, 11584–11585.
60 C. Poon, C. He, D. Liu, K. Lu, and W. Lin, *J. Control. Release*, 2015, **201**, 90–99.
61 R. C. Huxford, K. E. DeKrafft, W. S. Boyle, D. Liu, and W. Lin, *Chem. Sci.*, 2012, **3**, 198–204.
62 L. Xing, Y. Cao, and S. Che, *Chem. Commun.*, 2012, **48**, 5995–5997.
63 L. Zhang, X. Qian, L. Liu, Z. Shi, Y. Li, S. Wang, H. Liu, and Y. Li, *Chem. Commun.*, 2012, **48**, 6166–6168.
64 Y. Yang, Q. Hu, Q. Zhang, K. Jiang, W. Lin, Y. Yang, Y. Cui, and G. Qian, *Mol. Pharm.*, 2016, **13**, 2782–2786.
65 J. An, S. J. Geib, and N. L. Rosi, *J. Am. Chem. Soc.*, 2009, **131**, 8376–8377.
66 R. Anand, F. Borghi, F. Manoli, I. Manet, V. Agostoni, P. Reschiglian, R. Gref, and S. Monti, *J. Phys. Chem. B*, 2014, **118**, 8532–8539.
67 S. Turner, O. I. Lebedev, F. Schröder, D. Esken, R. a Fischer, and G. Van Tendeloo, *Chem. Mater.*, 2008, **20**, 5622–5627.
68 Q.-L. Zhu, J. Li, and Q. Xu, *J. Am. Chem. Soc.*, 2013, **135**, 10210–10213.
69 K. A. Mkhoyan, A. W. Contryman, J. Silcox, D. A. Stewart, G. Eda, C. Mattevi, S. Miller, and M. Chhowalla, *Nano Lett.*, 2009, **9**, 1058-1063.
70 S. Schmitt, M. Silvestre, M. Tsotsalas, A. L. Winkler, A. Shahnas, S. Grosjean, F. Laye, H. Gliemann, J. Lahann, S. Bräse, M. Franzreb, and C. Wöll, *ACS Nano*, 2015, **9**, 4219–4226.
71 J. Zhou, P. Wang, C. Wang, Y. T. Goh, Z. Fang, P. B. Messersmith, and H. Duan, *ACS Nano*, 2015, **9**, 6951–6960.
72 K. Deng, Z. Hou, X. Li, C. Li, Y. Zhang, X. Deng, Z. Cheng, and J. Lin, *Sci. Rep.*, 2015, **5**, 7851–7855.
73 K. Suenaga, Y. Sato, Z. Liu, H. Kataura, T. Okazaki, K. Kimoto, H. Sawada, T. Sasaki, K. Omoto, T. Tomita, T. Kaneyama, and Y. Kondo, *Nat. Chem.*, 2009, **1**, 415–418.
74 B. W. Smith, M. Monthioux, and D. E. Luzzi, *Nature*, 1998, **396**, 323–324.
75 A. N. Khlobystov, D. a Britz, and G. A. D. Briggs, *Acc. Chem. Res.*, 2005, **38**, 901–909.
76 M. Koshino, T. Tanaka, N. Solin, K. Suenaga, H. Isobe, and E. Nakamura, *Science*, 2007, **316**, 853–853.
77 Z. Liu, X. Sun, N. Nakayama-Ratchford, and H. Dai, *ACS Nano*, 2007, **1**, 50–56.
78 R. Li, R. Wu, L. Zhao, Z. Hu, S. Guo, X. Pan, and H. Zou, *Carbon N. Y.*, 2011, **49**, 1797–1805.
79 M. Prato, K. Kostarelos, and A. Bianco, *Acc. Chem. Res.*, 2008, **41**, 60–68.
80 D. Pantarotto, R. Singh, D. McCarthy, M. Erhardt, J.-P. Briand, M. Prato, K. Kostarelos, and A. Bianco, *Angew. Chemie Int. Ed.*, 2004, **43**, 5242–5246.
81 A. K. Varkouhi, S. Foillard, T. Lammers, R. M. Schiffelers, E. Doris, W. E. Hennink, and G. Storm, *Int. J. Pharm.*, 2011, **416**, 419–425.
82 D. Pantarotto, C. D. Partidos, J. Hoebeke, F. Brown, E. Kramer, J.-P. Briand, S. Muller, M. Prato, and A. Bianco, *Chem. Biol.*, 2003, **10**, 961–966.
83 J. Li, S. Q. Yap, S. L. Yoong, T. R. Nayak, G. W. Chandra, W. H. Ang, T. Panczyk, S. Ramaprabhu, S. K. Vashist, F. S. Sheu, A. Tan, and G. Pastorin, *Carbon*, 2012, **50**, 1625–1634.
84 A. W. Robertson and J. H. Warner, *Nanoscale*, 2013, **5**, 4079–4093.
85 P. Y. Huang, C. S. Ruiz-Vargas, A. M. van der Zande, W. S. Whitney, M. P. Levendorf, J. W. Kevek, S. Garg, J. S. Alden, C. J. Hustedt, Y. Zhu, J. Park, P. L. McEuen, and D. A. Muller, *Nature*, 2011, **469**, 389–392.
86 O. L. Krivanek, M. F. Chisholm, V. Nicolosi, T. J. Pennycook, G. J. Corbin, N. Dellby, M. F. Murfitt, C. S. Own, Z. S. Szilagyi, M. P. Oxley, S. T. Pantelides, and S. J. Pennycook, *Nature*, 2010, **464**, 571–574.
87 K. Suenaga and M. Koshino, *Nature*, 2010, **468**, 1088–1090.
88 A. Tararan, A. Zobelli, A. M. Benito, W. K. Maser, and O. Stéphan, *Chem. Mater.*, 2016, **28**, 3741–3748.
89 K. A. Mkhoyan, A. W. Contryman, J. Silcox, D. A. Stewart, G. Eda, C. Mattevi, S. Miller, and M. Chhowalla, *Nano Lett.*, 2009, **9**, 1058–1063.
90 X. Sun, Z. Liu, K. Welsher, J. T. Robinson, A. Goodwin, S. Zaric, and H. Dai, *Nano Res.*, 2008, **1**, 203–212.
91 Z. Liu, J. T. Robinson, X. Sun, and H. Dai, *J. Am. Chem. Soc.*, 2008, **130**, 10876–10877.
92 W. Miao, G. Shim, G. Kim, S. Lee, H. J. Lee, Y. B. Kim, Y. Byun, and Y. K. Oh, *J. Control. Release*, 2015, **211**, 28–36.
93 S. Moradi, O. Akhavan, A. Tayyebi, R. Rahighi, M. Mohammadzadeh, and H. R. Saligheh Rad, *RSC Adv.*, 2015, **5**, 47529–47537.
94 S. Gao, L. Zhang, G. Wang, K. Yang, M. Chen, R. Tian, Q. Ma, and L. Zhu, *Biomaterials*, 2016, **79**, 36–45.

View Article Online
DOI: 10.1039/C6TB03062A

95 K. Yang, J. Wan, S. Zhang, Y. Zhang, S. T. Lee, and Z. Liu, *ACS Nano*, 2011, **5**, 516–522.
96 D. Moazed, *Nature*, 2009, **457**, 413–420.
97 J. Joo, E. J. Kwon, J. Kang, M. Skalak, E. J. Anglin, A. P. Mann, E. Ruoslahti, S. N. Bhatia, and M. J. Sailor, *Nanoscale Horiz.*, 2016, **1**, 407–414.
98 J. T. Robinson, S. M. Tabakman, Y. Liang, H. Wang, H. Sanchez Casalongue, D. Vinh, and H. Dai, *J. Am. Chem. Soc.*, 2011, **133**, 6825–6831.
99 G. Gonçalves, M. Vila, M. T. Portolés, M. Vallet-Regi, J. Gracio, and P. A. A. P. Marques, *Adv. Healthc. Mater.*, 2013, **2**, 1072–1090.
100 Z.-M. Wang, W. Wang, N. Coombs, N. Soheilnia, and G. a Ozin, *ACS Nano*, 2010, **4**, 7437–7450.
101 Y. Wang, K. Wang, J. Zhao, X. Liu, J. Bu, X. Yan, and R. Huang, *J. Am. Chem. Soc.*, 2013, **135**, 4799–4804.
102 B. Díaz, C. Sánchez-Espinel, M. Arruebo, J. Faro, E. De Miguel, S. Magadán, C. Yagüe, R. Fernández-Pacheco, M. R. Ibarra, J. Santamaría, and Á. González-Fernández, *Small*, 2008, **4**, 2025–2034.
103 A. K. Gupta and M. Gupta, *Biomaterials*, 2005, **26**, 3995–4021.
104 S. Asahina, T. Togashi, O. Terasaki, S. Takami, T. Adschiri, M. Shibata, and and N. Erdman, *Microsc. Anal.*, 2012, **26**, S12–S14.
105 M. Havrdova, K. Polakova, J. Skopalik, M. Vujtek, A. Mokdad, M. Homolkova, J. Tucek, J. Nebesarova, and R. Zboril, *Micron*, 2014, **67**, 149–154.
106 G. Plascencia-Villa, C. R. Starr, L. S. Armstrong, A. Ponce, and M. José-Yacamán, *Integr. Biol. (Camb).*, 2012, **4**, 1358–1366.
107 N. Liv, D. S. B. van Oosten Slingeland, J.-P. Baudoin, P. Kruit, D. W. Piston, and J. P. Hoogenboom, *ACS Nano*, 2016, **10**, 265–273.
108 Y. Zhao, X. Sun, G. Zhang, B. G. Trewyn, I. I. Slowing, and V. S.-Y. Lin, *ACS Nano*, 2011, **5**, 1366–1375.
109 B. M. Rothen-Rutishauser, S. Schürch, B. Haenni, N. Kapp, and P. Gehr, *Environ. Sci. Technol.*, 2006, **40**, 4353–4359.
110 T. G. Iversen, T. Skotland, and K. Sandvig, *Nano Today*, 2011, **6**, 176–185.
111 G. Sahay, D. Y. Alakhova and A. V. Kabanov, *J. Control. Release*, 2010, **145**, 182–195.
112 H. M. Ding and Y. Q. Ma, *Biomaterials*, 2012, **33**, 5798-5802.
113 W. Jiang, B. Y. S. Kim, J. T. Rutka, and W. C. W. Chan, *Nat. Nanotechnol.*, 2008, **3**, 145–150.
114 E. Callaway, *Nature*, 2015, **525**, 172-174
115 E. Binshtein and M. D. Ohi, *Biochemistry* 2015, **54**, 3133−3141
116 F. M. Ross, *Science*, 2015, **350**, 1490.
117 D. B. Peckys and N. de Jonge, *Nano Lett.*, 2011, **11**, 1733–1738.

View Article Online
DOI: 10.1039/C6TB03062A

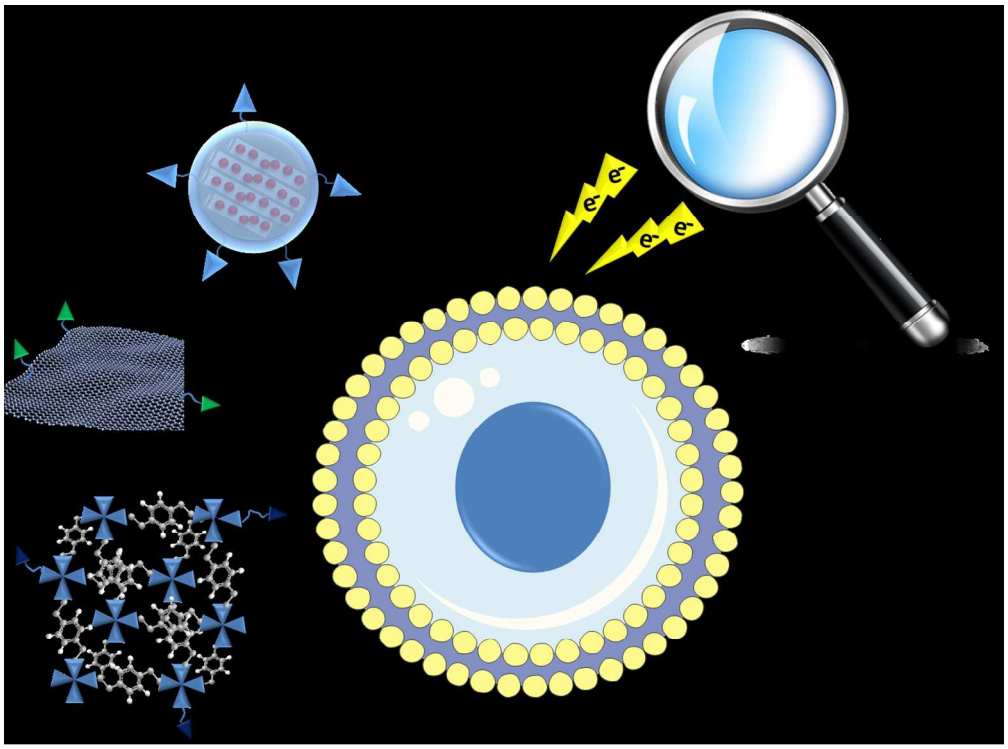

257x189mm (150 x 150 DPI)